35th EPS Conference on Plasma Phys. Hersonissos, 9 - 13 June 2008 ECA Vol.**32D**, D-5.011 (2008)

Correlative Enhanced Scattering Diagnostics in Dense Magnetized Plasmas

A.B. Altukhov[1], A.D. Gurchenko[1], E.Z. Gusakov[1], M. Krämer[2]

[1] *Ioffe Institute, St. Petersburg, Russian Federation*
[2] *Institut für Experimentalphysik II, Ruhr-University Bochum, Germany*

1. Introduction

The correlative enhanced scattering (CES) technique has been recently successfully applied for studying the drift-wave turbulence in tokamak [1], in particular, evidencing ETG mode excitation for the first time. This technique utilizes *X* mode microwave probing at the upper hybrid resonance (UHR), which is accessible from the high magnetic field (MF) side of the torus for standard tokamak, where the electron cyclotron frequency is higher than the central electron plasma frequency, $\omega_{ce} > \omega_{pe}(0)$. In contrast, in spherical tokamaks (ST) operating at relatively low MF and high density, the opposite condition $\omega_{ce} < \omega_{pe}(0)$ holds. Although the UHR surface is then inaccessible, significant coupling of the microwave power to the UHR from the low MF side can be achieved if $\omega_{ce} << \omega_{pe}(0)$ and the evanescent region between the cutoff and the UHR is thus very narrow [2, 3], as it is typical for ST (Fig.1).

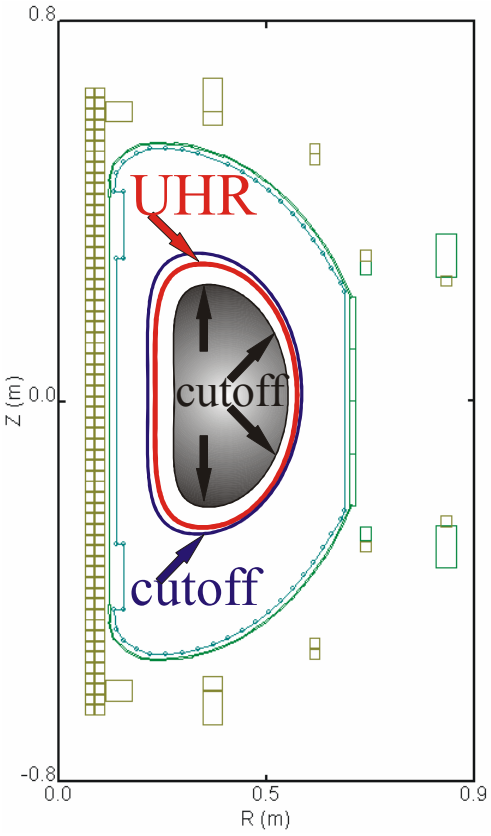

Fig. 1. UHR and cutoff layers for X mode wave in tokamak Globus-M.

2. Experiment and Results

The feasibility of the CES scheme for determining turbulence wave number (q) spectra in high-density magnetized plasma is studied on the helicon source HE-L having similar electromagnetic properties as ST [2]. The plasma (radius $r_p = 73$ mm, length $L_p = 1.1$ m) is produced by *rf* power pulses ($P_{rf} \leq 2$ kW, $f_{rf} = 13.56$ MHz, $\tau_{pulse} = 3$-5 ms, $f_{pulse} = 50$ Hz) through an helical antenna. The small-scale plasma density fluctuations excited by the *rf* fields are diagnosed for high-density conditions ($\omega_{pe} >> \omega_{ce}$) so that the UHR frequency $\omega_{UH} \approx \omega_{pe}$. Despite strong reflection of the probing wave at the cutoff, the ES signal is high enough to be detected. Unlike [2], where only the real part of the CES cross-correlation

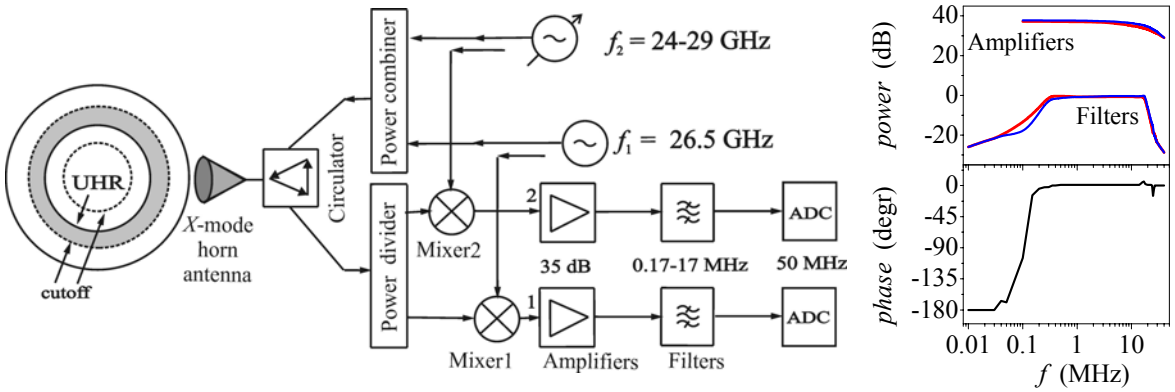

Fig. 2. CES scheme and frequency characteristics for amplifiers and filters.

function (CCF) was directly measured, the complex CCF is here computed, and the radial wave number q_R spectra are reconstructed from these measurements using the approach employed in [1]. The cross-correlation scheme (Fig. 2a) has two homodyne channels with probing frequencies f_1 and f_2. The probing and receiving waveguides are separated by a microwave circulator. The back-scattered signals after 35 dB amplification are filtered out by 7-order low-pass and 3-order high-pass filters (frequency characteristics of amplitude and phase shown in Fig. 2b), stored by a 12-bit data acquisition system (DCO & PC). The microwave source with fixed frequency $f_1 = 26.5$ GHz defines the reference UHR position, depending on the density profile (Fig. 3). The low-frequency output of the mixer 1, employed for homodyne detection, corresponds to the scattered signal from the reference UHR position. The frequency of the second generator f_2 varies in the 24 - 29 GHz range.

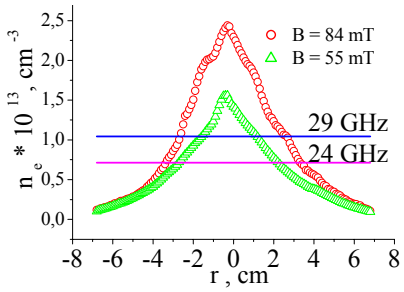

Fig. 3. Density profiles.

The scheme calibration implies phase matching between both channels: $\Delta\varphi = \varphi_1(f_1) - \varphi_2(f_2) = 0$, where $\varphi_1(f_1)$ and $\varphi_2(f_2)$ are the phase differences between the LO and receiving arms in the channels with constant and sweeping frequencies, respectively. With varying f_2 the phase φ_2 changes, but φ_1 remains constant. To provide $\varphi_2(f_2) = \varphi_2(f_1) + (\delta\varphi_2/\delta f_2)(f_2-f_1) =$ = const. it is necessary to nullify $(\delta\varphi_2/\delta f_2)$ so that the delay time between the signals in the receiving and LO arms become equal. This compensation is performed with a cable (C-cable) installed in the LO arm of the second homodyne channel. Thus, the variation of $\Delta\varphi$ is minimized; its value is turned to minimum by a phase shifter in the first homodyne channel.

The dependence of the Fourier transform of the CCF on the spatial separation of the UHR, which is proportional to the frequency difference f_1-f_2, provides the cross-correlation spectrum (CCS) of the ES signal. The CCS for $B_0 = 84$ mT and $p = 0.3$ Pa is shown in Fig. 4.

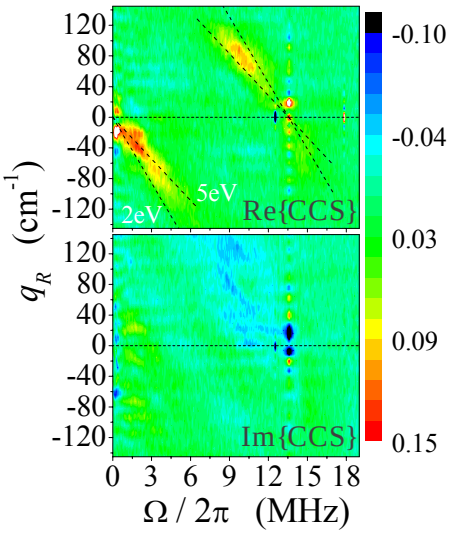

Fig. 4. CCS for B_0 = 84 mT.

The real and imaginary parts of the CCS (the latter is zero in theory) yield estimates of the signal and noise level, respectively.

As it is seen in Fig. 4, at low frequency $f_s - f_i < 6$ MHz the CCS prevails over the noise along the line $f_a = -q_R c_s/2\pi$, where $c_s \approx 3.8$ cm/s, corresponds to the ion-acoustic (IA) velocity at $T_e \approx 3$ eV. It allows identifying the low frequency (*lf*) waves, excited in the helicon discharge as IA waves, propagating to the discharge centre [2]. At higher frequencies the CCS rises along the parallel line $f_l = f_{rf} - q_R c_s/2R$. The phase velocity of these waves for $f_l < f_{rf}$ is directed to the plasma edge and, thus, opposite to the velocity of *lf* waves. The frequencies and radial wavenumbers of these waves satisfy the three-wave resonance conditions (TWRC) $f_l = f_{rf} - f_a$ and $q_l = -q_a$ that are characteristic for the parametric decay instability of a long-scale pump wave. The same picture, is not observed for $f_s - f_i < 1$ MHz. It is explained by the high level of small-angle scattering and by probing wave reflection (blue curve in Fig. 5.) which exists even without the UHR in the plasma. The black curve is the reflected signal without plasma and the red and green curves correspond to the ES signals for 55 and 84 mT regimes. It is clearly seen in Fig. 5b that the ES signal is dominant for $|f_s - f_i| > 1$ MHz.

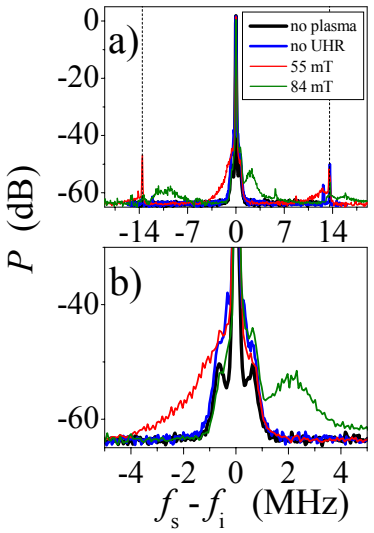

Fig. 5. Super-heterodyne spectra.

3. CES scheme calibration.

The influence of the scheme calibration on the proper measurements of the *lf* dispersion line was especially investigated. First experiments with the scheme in [2] were performed at 42 mT with a cable length $l_c = 24$ cm. In this case, the *lf* wave dispersion curve is shown by yellow triangles in Fig. 6 and approximation line 4, where it does not cross the origin of the coordinate system (OC), as it should hold for IA waves. Taking into account the real shape of the profile, the C-cable was increased to 36 cm and the dispersion line intersects OC (blue symbols and line 3

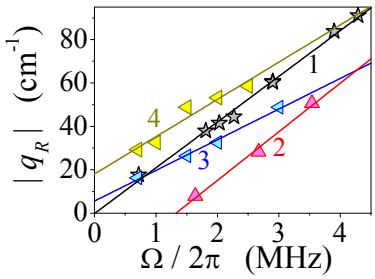

Fig. 6. Dispersion curves for LF spectral component measured by ES: 1 – 84 mT, l_c = 30 cm; 2 – 84 mT, 36 cm; 3 – 42 mT, 36 cm, 4 – 42 mT, 24 cm.

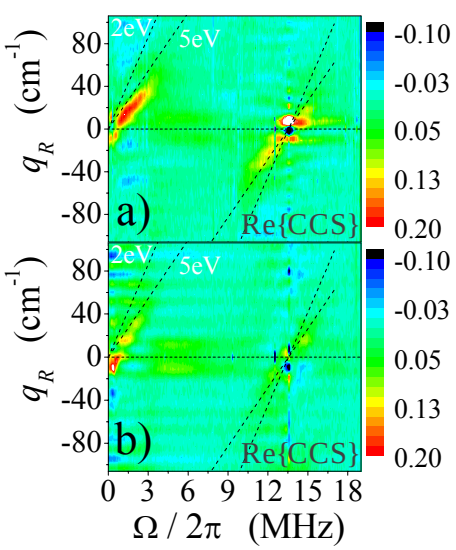

Fig. 7. CCS for 55 mT with a) equatorial and b) down shifted probing.

in Fig. 6). However, the points measured with this calibration in the high-field regime (B_0 = 84 mT) do not cross OC again (red symbols, line 2). This can be explained by variation of the density profiles causing the distance between the plasma edge and the UHR to change. The excellent calibration which resulted in Fig.4 was obtained in that regime with a 30 cm C-cable (black stars, line 1 for lf wave in Fig 6). That the proper calibration of the correlation scheme is important to confirm the decay conditions is shown for B_0 = 55mT where the real part of the CCS was measured with latter cable (see fig.7a). It should be stressed that although the difference between UHR positions at the profiles for 55 mT and 84 mT is not very significant (< 1 cm; see Fig. 3), it was sufficient to distort the calibration. The *lf* wave dispersion line in this case does not intersect the OC again. It is shifted along the q_R axis by 10 cm^{-1}, whereas the *hf* wave line is shifted along the q_R axis in the opposite direction, thus making the decay condition matching impossible.

The CCS obtained for 55 mT when the antenna horn was down-shifted by $0.2r_p$ with respect to the equatorial plane keeping the central line of the antenna diagram parallel to it is shown in Fig. 7b. The drop of the ES signal level due to increase of the evanescent region width decreases the signal to noise ratio and leads to appearance of noise-like parasitic lines.

4. Conclusions

Detailed measurements of the ion-acoustic and oblique plasma wave turbulence spectra arising from the parametric decay instability of the helicon were performed with the CES diagnostics for different density profiles and probing antenna positions in a wide MF range. The efficiency of the CES scheme was demonstrated in the helicon discharge experiment possessing electromagnetic conditions similar to the spherical tokamak. The importance of the CES scheme calibration accounting for the finite path of the probing wave in the plasma was demonstrated.

Financial support from the RFBR grants 07-02-00746 and 08-02-90011-Bel_a, the DFG Contract 436 RUS 113/590 and the “Russian Science Support Foundation” is gratefully acknowledged.

[1] E.Z. Gusakov, A.D. Gurchenko, A.B. Altukhov, et al., *Plasma Phys. Control. Fusion* 48, A371 (2006)
[2] A.B. Altukhov, E.Z. Gusakov, M.A. Irzak, M.Krämer, B.Lorenz, V.Selenin, Phys.Plasmas 12, 22310 (2005)
[3] A D Piliya, E N Tregubova, *Plasma Phys. Control. Fusion* 47, 143 (2005)